RSC Pharmaceutics

ROYAL SOCIETY OF CHEMISTRY

PAPER

View Article Online
View Journal | View Issue

Cite this: *RSC Pharm.*, 2024, **1**, 458

Fabrication of miconazole nitrate solid lipid nanoparticle loaded microneedle patches for the treatment of *Candida albicans* biofilms

Muhammad Sohail Arshad,[a] Aqsa Ayub,[a] Saman Zafar,[a] Sadia Jafar Rana,[a] Syed Aun Muhammad,[b] Ambreen Aleem,[a] Ekhoerose Onaiwu,[c] Kazem Nazari,[c] Ming-Wei Chang[d] and Zeeshan Ahmad *[c]

The present study aimed to develop miconazole nitrate solid lipid nanoparticle (SLN) loaded polymeric microneedle (MN) patches (SPs) *via* the vacuum micromolding approach. The SLNs were fabricated through melt emulsification of stearic acid using Tween 80. SPs were prepared using chitosan, gelatin (as base materials) and polyethylene glycol 400 (as a plasticizer). The prepared formulations were evaluated for various physicochemical parameters, including particle size, polydispersity index, encapsulation efficiency, loading capacity (in the case of SLNs), folding endurance, % swelling and insertion ability (in the case of SPs). Scanning electron microscopy and differential scanning calorimetry (DSC) studies were carried out for morphological and thermal analysis, respectively. Phase analysis was carried out *via* X-ray diffraction (XRD). *In vitro* tensile strength, drug release, anti-biofilm activity and *in vivo* anti-biofilm activity were studied to assess the efficiency of the SLN loaded polymeric formulation. Miconazole nitrate containing SLNs appeared as smooth-surfaced aggregates and displayed a particle diameter of ~224 nm, polydispersity index of ~0.32, encapsulation efficiency of ~88.88% and loading capacity of ~8.88%. SPs exhibited evenly aligned, uniform-surfaced, sharp-tipped projections, with an acceptable folding endurance of ~300 and % swelling of ~359%. DSC and XRD results confirmed the incorporation of the drug within the solidified lipid matrix as an amorphous solid. The miconazole nitrate lipidic nanoparticle containing polymeric formulation exhibited a tensile strength ~1.35 times lower than the pure drug loaded counterpart. During *in vitro* studies, SPs released ~94% miconazole nitrate within 150 minutes and reduced the mass of the *Candida albicans* (*C. albicans*) biofilm by ~79%. After 10 days of treatment with SPs, *C. albicans* infected wounds were healed, confirming that the prepared formulations can be used for the management of fungal biofilms.

Received 11th February 2024,
Accepted 27th April 2024

DOI: 10.1039/d4pm00042k

rsc.li/RSCPharma

1. Introduction

Cutaneous wound healing is an organized sequential process comprising multiple events such as haemostasis, inflammation, granulation and remodelling.[1] This cascade of biological events is disturbed upon infiltration, proliferation and colonization of infectious microorganisms in the disrupted skin layers. These microbes release pro-inflammatory cytokines, which extend the inflammatory phase of the wounds. In most cases (~80%), mono- or poly-microbial (*e.g.*, fungi, bacteria, and viruses) aggregates (biofilms) develop at the injured site. The pathogens attach to the injured surface by producing a polysaccharide matrix and form a physical barrier.[2–4] Topical and systemic anti-microbial agents are commonly used for the treatment of biofilms. Barriers such as biofilms and necrotic tissue hamper the efficient delivery of conventional topical therapeutic agents (*e.g.*, creams, lotions, gels, and ointments), resulting in sub-therapeutic levels in the microbial microenvironment. Systemic anti-microbials are also unable to reach the infected site at therapeutic levels because of poor vascularization, thus promoting anti-microbial resistance.[1,4,5]

Various micro- or nano-scale multi-particulate carriers, *e.g.*, liposomes, polymeric nanoparticles, and solid lipid nanoparticles (SLNs), have been developed to overcome these limitations and ensure efficient administration of drugs to the desired site. These carriers are reported to protect the encapsulated active ingredient from degradation induced by proteases

[a]*Faculty of Pharmacy, Bahauddin Zakariya University, Multan, Pakistan*
[b]*Institute of Molecular Biology and Biotechnology, Bahauddin Zakariya University, Multan, Pakistan*
[c]*Leicester School of Pharmacy, De Montfort University, Leicester, UK. E-mail: zahmad@dmu.ac.uk*
[d]*Nanotechnology and Integrated Bioengineering Centre, University of Ulster, Jordanstown Campus, Newtownabbey BT37 0QB, Northern Ireland, UK*

present in the wound fluid, improve drug retention/residence time, modulate drug release and create a moist environment, thus accelerating the healing process. Amongst these carriers, SLNs are preferred due to their safety (as toxic solvents are not used during production), stability, avoidance of drug leakage (because of using lipids which are solid at room as well as body temperature) and cost-effectiveness (in terms of excipients and fabrication approaches).[6–10] Examples of solid lipids used for fabricating SLNs include tristearin, trimyristin, palmitic acid, glyceryl monostearate and cetyl palmitate. Stearic acid is a biocompatible saturated solid fatty acid with a melting point around 69 °C and thus can act as a base material for preparing SLNs.[11,12] Tween 80, a non-ionic hydrophilic surfactant with an HLB (hydrophilic lipophilic balance) value of 15, is generally recognized as safe and hence can be used to stabilize the SLN dispersion.[13–15] Drug containing SLNs can be loaded into suitable platforms, *e.g.*, polymeric microneedle (MN) patches and delivered to the desired cutaneous site.[16]

A MN patch comprises multiple micron-scale (25–2500 μm) projections arranged in a sequence.[17] The needles can breach the physical obstacles (biofilm, necrotic tissue, and cellular debris) in a minimally invasive manner and deliver the loaded therapeutic moiety within deep wound layers. MN mediated delivery ensures high bioavailability of loaded antibacterial/antifungal agents at the infected site and, in turn, a reduced risk of antimicrobial resistance. Dissolving MNs prepared using biocompatible, biodegradable and non-toxic polymers can serve as suitable candidates for delivering antimicrobial agents to the infected/injured site.[18–21] Chitosan (a polysaccharide) and gelatin (a polypeptide) interact *via* their amino and carboxyl groups, respectively, and form suitable hybrid matrices. These polymers can be used to fabricate MN patches due to their good film-forming abilities. Polyethylene glycol (PEG 400) is used as a plasticizing agent, which can reduce the brittleness and increase the flexibility of MN patches.[22]

Miconazole nitrate is a broad-spectrum imidazole derivative anti-fungal agent belonging to BCS (biopharmaceutical classification system) class II (highly permeable, poorly soluble). It is used to treat *Candida albicans* (*C. albicans*, one of the most common opportunistic fungal pathogens found in infected wounds) biofilms. This highly lipophilic agent exhibits low bioavailability in the skin strata; thus, lipid-based nanoparticles can enhance its on-site presence and serve as potential carriers for its transcutaneous delivery.[6,7,10,23,24]

The present study aimed to prepare miconazole nitrate SLN (comprising stearic acid and Tween 80) loaded MN patches (based on gelatin, chitosan and PEG 400) by using the vacuum micromolding approach. The prepared formulations were evaluated for *in vitro* drug release and anti-biofilm activity and *in vivo* anti-biofilm activity.

2. Materials and methods

2.1. Materials

Miconazole nitrate was gifted by Nabiqasim Industries Private Limited, Karachi, Pakistan. Stearic acid, Tween 80 and glacial acetic acid were purchased from Merck, Darmstadt, Germany. Gelatin was purchased from BDH, Poole, England. Chitosan was procured from MP Biomedicals, IllKirch-Graffenstaden, France. PEG-400, potassium phosphate monobasic and methanol were obtained from Duksan, Gyeonggi-do, South Korea. Sodium hydroxide was procured from Sigma Aldrich, Steinheim, Germany. Sabouraud dextrose broth was purchased from Lab M Limited, Heywood, United Kingdom. Distilled water was obtained from an in-house facility (Department of Pharmaceutics, Faculty of Pharmacy, Bahauddin Zakariya University, Multan, Pakistan).

2.2. Method of preparation

2.2.1. Preparation of solid lipid nanoparticles. SLNs were fabricated by the melt emulsification method. Briefly, the lipid phase (comprising stearic acid) and aqueous phase (comprising Tween 80 dissolved in distilled water [10–20% w/w solid lipid]) were heated individually at 77 ± 3 °C with continuous stirring for 5–10 minutes. The aqueous phase was gradually added to the molten lipid whilst stirring continuously. The formed emulsion was added to the cold distilled water followed by continuous stirring at 2–4 °C and 1000 rpm for ~3 hours to produce nanoparticles. The aqueous SLN dispersion was centrifuged at 6000 rpm for ~5 minutes. The supernatant was discarded, and sedimented SLNs were collected, dried at room temperature (25 ± 3 °C) and stored in a desiccator chamber until further use. For preparing miconazole nitrate loaded SLNs, the drug (10% w/w solid lipid) was mixed with the lipid phase and the nanoparticles were prepared by following the aforementioned protocol.

2.2.2. Preparation of solid lipid nanoparticle loaded films. Gelatin, chitosan and PEG 400 were dissolved in varying concentration, *i.e.*, 4–8% w/v, 0.5–2% w/v and 10–35% w/w polymeric mass, respectively, in 1% acetic acid solution with continuous stirring at 100 rpm for 10–12 hours. Miconazole nitrate loaded SLNs were mixed with the prepared optimized polymeric solution. For preparing the SLN loaded film (SF), miconazole nitrate nanoparticle loaded polymeric solution was poured into appropriate molds (10 × 10 mm) and kept at 25 ± 3 °C for 48–72 hours. Upon drying, the films were detached from the molds and stored in air-tight containers until further use.

As control formulations, blank, *i.e.*, without drug (BF, negative control) and pure anti-fungal agent loaded films (MF, positive control) were fabricated. The BF was prepared by pouring the gelatin, chitosan and PEG 400-based polymeric solution in molds followed by incubation at 25 ± 3 °C for ~48 hours and detachment upon drying. For the MF, a methanolic solution of miconazole nitrate (10% w/w polymeric mass) was added to the polymeric solution, poured in molds and incubated at 25 ± 3 °C. After ~48 hours, the dried films were separated from molds.

2.2.3. Preparation of solid lipid nanoparticle loaded microneedle patches. Stainless steel master molds of different needle sizes, *i.e.*, 150 μm, 300 μm and 500 μm were engineered by traditional machining methods including grinding, electro-

discharge process and electropolishing. A mixture comprising Dow Corning Sylgard 184 silicone and hardener (9 : 1) was poured to the prepared master molds and heated at 80 ± 3 °C for ~60 minutes. The polydimethylsiloxane (PDMS) MN molds were detached from the master molds upon curing.

The miconazole nitrate SLN loaded optimized polymeric solution was added to the PDMS molds, and placed in a vacuum chamber (600 mm of Hg) for 2–3 hours followed by incubation at room temperature (25 ± 3 °C). After ~72 hours, the dried polymeric MN patches (SP) were separated from PDMS molds and stored at room temperature until further use.

2.3. Physicochemical evaluation of solid lipid nanoparticles

Physicochemical evaluation of SLNs comprised determination of average diameter, polydispersity index, encapsulation efficiency and loading capacity. Average diameter and polydispersity index of blank and miconazole nitrate loaded SLNs were estimated by photon correlation spectroscopy using a Zetasizer (Malvern Panalytical, Malvern, United Kingdom). The samples were dispersed in distilled water and the particle size measurement was performed at 25 ± 2 °C. The encapsulation efficiency and loading capacity were determined by centrifuging the aqueous dispersion of SLNs at 12 000 rpm for 15 minutes. The supernatant was diluted with methanol, absorbance at λ_{max} 272 nm was recorded by using a UV-visible spectrophotometer (Hitachi, Tokyo, Japan) and the amount of free drug was determined. Encapsulation efficiency (%) and loading capacity (%) were calculated by using eqn (1) and (2), respectively.[25]

$$\text{Encapsulation efficiency}(\%) = \frac{\text{Loaded drug} - \text{Free drug}}{\text{Loaded drug}} \times 100 \quad (1)$$

$$\text{Loading capacity}(\%) = \frac{\text{Loaded drug} - \text{Free drug}}{\text{Loaded lipid}} \times 100 \quad (2)$$

2.4. Physicochemical evaluation of solid lipid nanoparticle loaded films and microneedle patches

The prepared formulations including BF, MF, SF and SP were evaluated for physical appearance, thickness, width, folding endurance and % swelling. The formulations were physically examined with the help of images captured by using a digital camera (Samsung, Seoul, South Korea). The thickness and width of prepared formulations (N = 10) were measured using a digital vernier caliper (Lufen, Zhejiang, China). For estimating folding endurance, the polymeric formulations (N = 10) were repeatedly folded at the same position until the structural integrity was lost.

Polymeric formulations (N = 5) of known mass (Mi) were individually placed into Petri plates containing phosphate buffer (pH 7.4). At specified time intervals, the swollen formulations were removed and weighed. The formulations were re-submerged in the buffer and the procedure was repeated until a constant mass (M_f) was obtained. Swelling (%) was calculated by using eqn (3).

$$\text{Swelling}(\%) = \frac{M_f - M_i}{M_i} \times 100 \quad (3)$$

In the case of the SP formulation, an *in vitro* insertion study (on skin simulant parafilm) and optical microscopy were also performed. For determining insertion ability, the SP was applied on the flexible parafilm (2 × 2 cm) by using thumb pressure for 40–45 seconds. The SP was removed and the treated film was examined under a light microscope (Labomed, Los Angeles, United States of America) at 40× resolution. The SP was placed on a glass slide and examined under an optical microscope at 40× resolution.

2.5. Scanning electron microscopy

Field emission scanning electron microscopy (Zeiss, Oberkochen, Germany) was employed to observe the surface morphology of miconazole nitrate and fabricated formulations including SLNs and SP. The formulations were individually placed on carbon stubs and coated with graphene (up to ~10 nm thickness) to improve image resolution. The photographs were recorded using FESEM and diameter/size as well as morphological features were analyzed.

2.6. Fourier transform infrared spectroscopy

Fourier transform infrared (FTIR) spectroscopy was performed at room temperature, *i.e.*, 25 ± 3 °C to investigate the interactions and compatibility between formulation constituents. The samples including miconazole nitrate SLNs, nanoparticle loaded polymeric formulation and their constituents were individually placed on the stage of the spectrophotometer (Bruker Alpha, Massachusetts, United States of America) and exposed to infrared radiation. The spectra were recorded as wave number (650–4000 cm^{-1}) *versus* transmittance at a resolution of 2 cm^{-1}.

2.7. Differential scanning calorimetry

The thermal analysis of stearic acid, miconazole nitrate, gelatin, chitosan, fabricated SLNs and nanoparticle loaded polymeric formulations was carried out with the help of a differential scanning calorimeter (DSC, TA Instruments, Delaware, United States of America). The samples (~10 mg) were individually transferred to alumina pans followed by heating over a temperature range of 35–300 °C at a rate of 10 °C per minute. The enthalpic changes were recorded as a function of temperature. Nickel was used to calibrate the instrument for temperature and heat flow under nitrogen gas purge at a rate of 50 ml per minute.

2.8. X-ray diffraction

Phase analysis of prepared drug loaded SLNs, miconazole nitrate SLN loaded polymeric formulations and their constituents was conducted using an X-ray diffractometer (XRD, D8 Discover, Bruker, Karlsruhe, Germany) at 40 kV and 40 mA.

The samples were added in the sample holder, mounted on the stage and scanned from 10° to 40° at a rate of 0.04°.

2.9. Mechanical properties

Mechanical properties of prepared formulations BF, MF and SF with specified dimensions (length 50 mm, width 10 mm) were assessed in terms of tensile strength, *i.e.*, the force required to break the polymeric strips to a point. Each strip was held, individually, between an upper stationary clamp and a lower moveable counterpart. The film strip was dragged apart by the lower clamp at a speed of 2 mm per second and trigger load of 0.05 Newton. Tensile strength was estimated using eqn (4).[26]

$$\text{Tensile strength} = \frac{\text{Force required to break polymeric strip(Newton)}}{\text{Initial cross sectional area(mm}^2\text{)}} \quad (4)$$

2.10. *In vitro* drug release study

For quantification of miconazole nitrate, the prepared formulations including MF, SF and SP were individually stirred at 100 rpm in a water-circulated flow cell (maintained at 37 ± 2 °C) containing 10 ml phosphate buffer (pH 7.4). At predetermined time intervals, *i.e.*, 15, 30, 45, 60, 80, 100, 120, 150 and 180 minutes, aliquots (1 ml) were withdrawn from the dissolution medium and an equal volume of blank phosphate buffer was introduced in the medium to maintain sink conditions. Aliquots were diluted with blank phosphate buffer, absorbance at λ_{max} 272 nm was recorded by using an ultraviolet-visible spectrophotometer and % release of miconazole nitrate from each formulation was calculated. The release profiles were analyzed by several dissolution models including zero order, first order, Higuchi, Korsmeyer-Peppas and Hixson Crowell.

2.11. *In vitro* anti-biofilm activity

Crystal violet assay was performed to assess the *in vitro* anti-biofilm activity of prepared formulations including BF, MS (aqueous suspension of miconazole nitrate, 1% w/v), SF and SP.[27–29] Briefly, sabouraud dextrose broth medium (3% w/v aqueous solution) was inoculated with *C. albicans* (ATCC 10231) and incubated at 37 ± 1 °C for ~24 hours. This inoculated medium (containing 1×10^7 cells per ml of *C. albicans*) was transferred to a 24-well microplate and incubated at 37 ± 1 °C for developing the biofilm. After ~24 hours, the medium was discarded and the microplate was rinsed with normal saline to remove the planktonic fungi. The formulations, *i.e.*, BF, MS, SF and SP were applied to the fungal biofilms with subsequent addition of normal saline and incubation at 37 ± 1 °C for ~24 hours. The liquid was discarded and wells were washed with normal saline followed by the addition of crystal violet reagent (0.1% w/v aqueous solution). The reagent was discarded after 15 ± 1 minutes and wells were rinsed with normal saline to remove the unbound dye. Ethanol (95%) was poured in order to dissolve the dye. Absorbance (Abs) was recorded at λ_{max} 595 nm by using a microplate reader (BioTek 800Ts Winooski, Vermont, United States of America). Reduction (%) in the biomass of *C. albicans* biofilms was estimated with the help of eqn (5) and the results were compared with the control (untreated fungal biofilms).

$$\%\text{Reduction} = \frac{\text{Abs}_{\text{control}} - \text{Abs}_{\text{treated}}}{\text{Abs}_{\text{control}}} \times 100 \quad (5)$$

2.12. *In vivo* anti-biofilm activity

All animal studies were approved by the Pharmacy Ethical Committee of Bahauddin Zakariya University Multan *vide* letter number 216/PEC/2022 and performed in accordance with the "Guide for the Care and Use of Laboratory Animals of the Institute for Laboratory Animal Research, US National Research Council of the National Academies".[30] Wistar albino rats (average weight 150–250 grams) were housed at room temperature (25 ± 2 °C) under a 12 : 12 light–dark cycle and given free access to food and water.

The rats were anesthetized by injecting ketamine (40 mg kg^{-1}) *via* the intra-peritoneal route and abdominal hairs were removed by using a chemical depilatory. An incision (~2 cm) was made using a sterile surgical blade (No. 12). *C. albicans* suspension (1×10^7 cells per ml) was poured over the incised skin. Samples were obtained daily from the wounded site by swabbing, heat-fixed on glass slides, stained with crystal violet and observed under an optical microscope (at 100× resolution) to observe the presence of *C. albicans* in the biofilm.

The animals ($N = 20$) were equally divided into four groups (labelled as BF, MS, SF and SP). After development of fungal biofilm, the formulations, *i.e.*, BF, MS, SF and SP were applied to the site of injury in the respective groups and the treatment was continued for 10 days. The infected sites were observed daily for wound healing. Furthermore, the sample was regularly taken from the incised skin, heat-fixed, stained and studied using a light microscope to observe the presence or absence of *C. albicans*.

On days 1 (biofilm development day), 6 and 10 of therapy, the skin tissues from each group were obtained by using a sterile surgical blade and fixed in 37% v/v formaldehyde. The skin tissues were sliced (1–2 μm thick) with the help of a microtome, placed on microscopic slides, hematoxylin and eosin-stained and examined using an optical microscope (at 40× magnification) for changes in skin structure following individual treatments.

3. Results

3.1. Physicochemical evaluation of solid lipid nanoparticles

A higher concentration of the surfactant, *i.e.*, Tween 80 (>10% w/w solid lipid) led to particle aggregation. The formulation comprising Tween 80 (10% w/w stearic acid) did not exhibit irregular aggregates, and thus was selected for further analysis. The nanoparticulate powder appeared white in color. Blank SLNs showed an average particle diameter and polydispersity

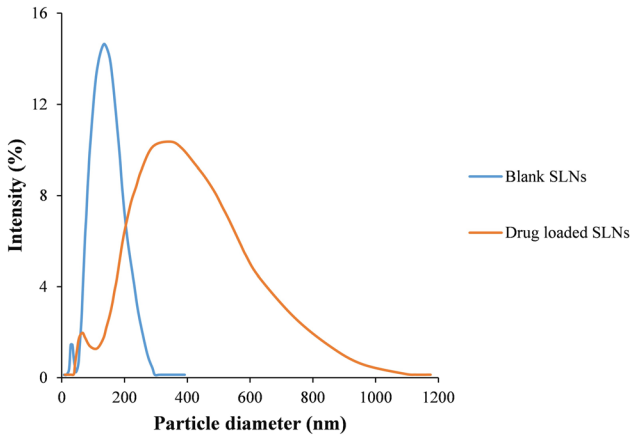

Fig. 1 Representative particle diameter/size distribution of blank and miconazole nitrate loaded SLNs.

index of ~104 nm and 0.171, respectively. In comparison, miconazole nitrate loaded SLNs exhibited a relatively larger particle diameter and higher polydispersity index, *i.e.*, ~224 nm and 0.320, respectively. Fig. 1 shows the size distribution of blank and miconazole nitrate incorporated SLNs. The blank formulation showed a relatively narrow distribution, suggesting uniformity of particle size as compared to drug loaded SLNs. The particle size at peak was 129.2 ± 44.65 nm and 352.3 ± 165.1 nm for blank and miconazole nitrate containing SLNs, respectively. The increase in diameter and polydispersity index was attributed to encapsulation of the drug within the SLNs. The proportion (% w/w polymeric mass) of miconazole nitrate responsible for % increase in the particle diameter remains a subject of future study. The encapsulation efficiency and loading capacity of prepared SLNs were found to be 88.88 ± 1.20% and 8.88 ± 0.11%, respectively.

3.2. Physicochemical evaluation of solid lipid nanoparticle loaded films and microneedle patches

The control (*i.e.*, BF and MF) and SLN loaded polymeric formulations (*i.e.*, SF and SP) containing low concentrations of gelatin and chitosan, *i.e.*, <4% w/v, and <1% w/v, respectively, were brittle and showed compromised structural integrity upon handling. The solution containing higher contents of gelatin and chitosan, *i.e.*, >6% w/v and ≥1.8% w/v was very viscous and difficult to mold. The formulations prepared from 5% w/v gelatin and 1% w/v chitosan showed an acceptable folding endurance (~100) and morphology. The formulations fabricated with a low concentration of PEG 400 (≤20% w/w polymeric mass) were fragile. The formulations containing a higher content of PEG 400 (>30% w/w polymeric mass) were malleable. Formulations containing 300% w/w polymeric mass PEG 400 exhibited acceptable structural integrity/folding endurance (~300). The optimized formulation comprising 5% w/v gelatin, 1% w/v chitosan and 30% w/w polymeric mass PEG 400 was analyzed in the next part of this study.

The prepared formulations showed a smooth, transparent surface (Fig. 2A and B, respectively), and an average thickness and width of ~0.88 ± 0.022 mm and ~8 ± 0.15 mm, respectively. The formulations were successfully folded ~300 ± 28 times without cracking, indicating structural integrity of the fabricated polymeric formulations. A swelling percentage of ~359 ± 17% suggested that the prepared polymeric formulations would efficiently uptake physiological fluid, which in turn would help in mass transfer.

Optical microscopy images of SP revealed evenly distributed and uniformly surfaced MNs (Fig. 2C). During the insertion study, the needle marks were successfully embossed on the parafilm. Clearly visible imprints of micron-scale structures on the model skin parafilm reflected the piercing ability of engineered MN devices. This suggested that the fabricated MN patches would breach the skin barrier and deliver the incorporated anti-fungal agent (Fig. 2D).

3.3. Scanning electron microscopy

The SEM images of miconazole nitrate, prepared SLNs and SP are depicted in Fig. 3. The SEM images of miconazole nitrate exhibited micron-scale (2.3 ± 1.5 μm) irregular shaped blocks. The spherical-shaped SLNs appeared as aggregates/clusters, while the isolated particles exhibited a uniform surface, suggesting sufficient mixing of the lipid, surfactant and drug. The SP showed sharp-tipped needles which would possibly breach the physical barriers and deliver miconazole nitrate in deep skin strata. The size of needles recovered was ~80% of PDMS mold specifications, *e.g.*, MNs prepared by using a 300 μm mold displayed a height of 240 ± 4 μm. The patch/needles exhibited an irregular, rough surface with sub-micron sized bead-like entities, which indicated the incorporation of SLNs into the polymeric MN patch.

3.4. Fourier transform infrared spectroscopy

The FTIR spectra of individual constituents and prepared formulations are represented in Fig. 4. Characteristic bands in the FTIR spectra indicate the vibrations of specific functional groups. The bands from all spectra are summarized in Table 1. The FTIR spectrum of anti-fungal agent loaded SLNs exhibited vibrational bands of stearic acid with a slight shift, which suggested the incorporation of Tween 80 and miconazole nitrate. The spectrum of the SLN encapsulated polymeric formulation manifested the vibrational bands of stearic acid, gelatin and chitosan (due to their abundance in the formulation) with slight shifts, indicating the incorporation of the surfactant, plasticizer, and drug and interaction between formulation constituents.

3.5. Differential scanning calorimetry

The DSC thermograms of prepared formulations and their constituents are shown in Fig. 5. In the thermal scan of miconazole nitrate, endothermic and exothermic peaks were observed at 189.20 °C and 213.58 °C, respectively, due to its melting and decomposition.[31,32] In the DSC thermogram of stearic acid, endothermic peaks at 61.12 °C and 301.88 °C rep-

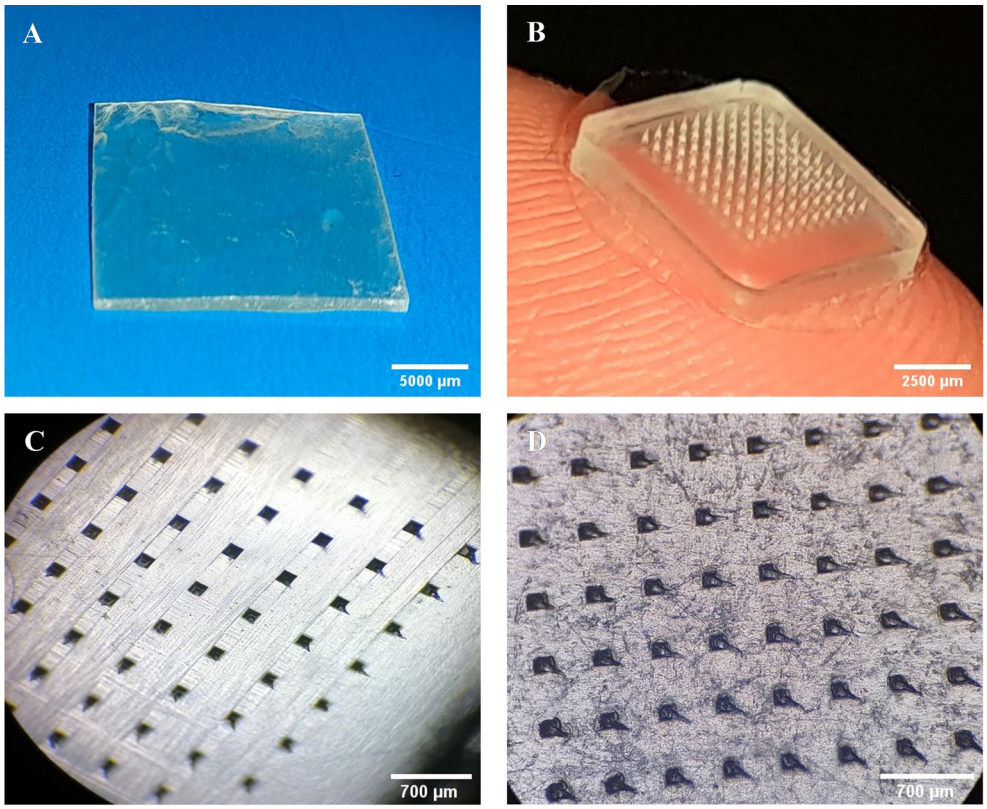

Fig. 2 Physical images of (A) the SF and (B) SP; microscopic images of (C) the SP and (D) SP treated parafilm.

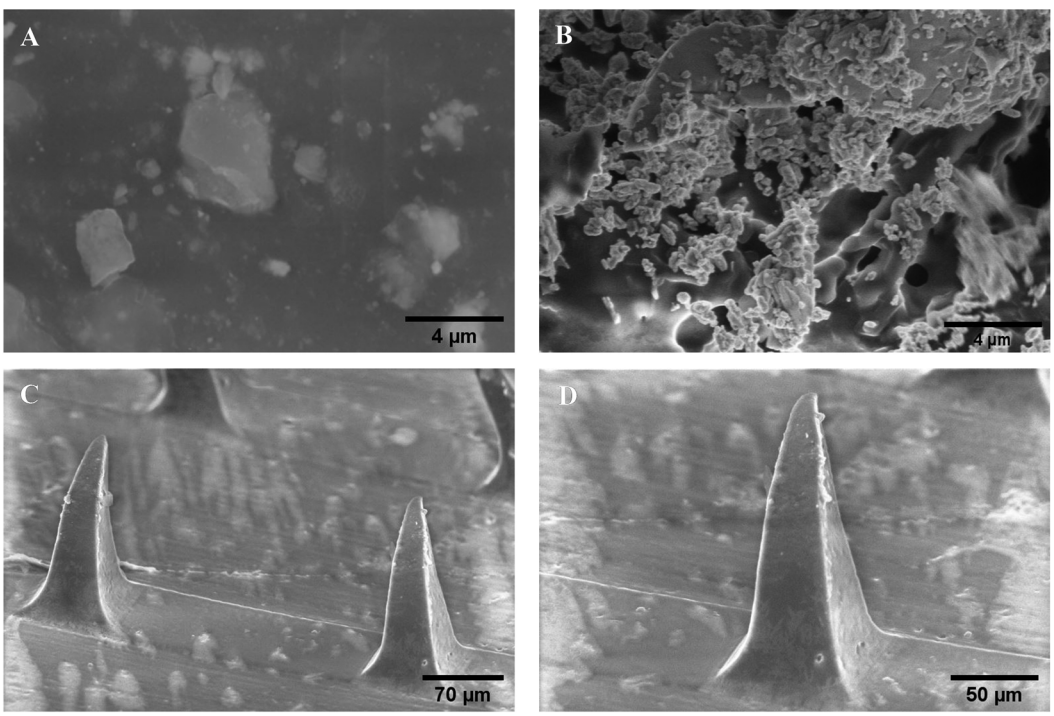

Fig. 3 Scanning electron microscopy images of (A) miconazole nitrate, (B) SLNs and SP at (C) 184× and (D) 300× magnification.

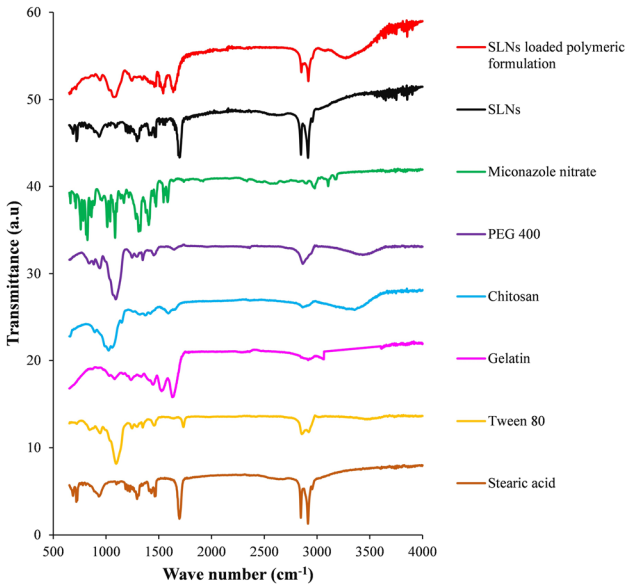

Fig. 4 Fourier transform infrared spectra of individual constituents, prepared miconazole nitrate SLNs and SLN loaded polymeric formulation.

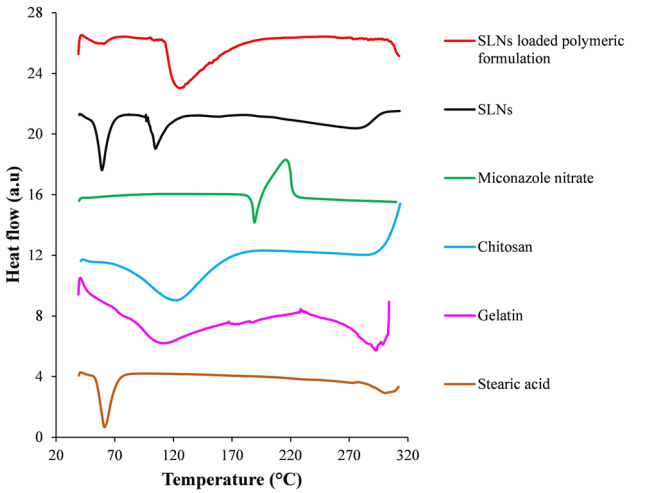

Fig. 5 Differential scanning calorimetry thermograms of individual components, prepared miconazole nitrate SLNs and SLN loaded polymeric formulation.

resented its melting and decomposition, respectively.[33,34] In the DSC scan of SLNs, two sharp endotherms at 59.10 °C and 104.64 °C suggested the melting and flash point (lowest temperature at which a liquid may form an ignitable mixture in the air) of stearic acid and Tween 80, respectively.[35,36] A broad endotherm at 265–285 °C was attributed to the degradation of stearic acid. As compared to pure ingredients, these events shifted to lower temperature values in the physical mixture possibly due to the adsorption of Tween 80 on the surface of SLNs.[6] The absence of melting endotherm of miconazole nitrate indicated the incorporation of the drug within the particles in an amorphous state.

In the thermal scan of chitosan, a broad endotherm over a temperature range of 68 °C–168 °C manifested the removal of water coupled with glass transition temperature. An exotherm onset around 290 °C suggested the decomposition of chitosan.[37] In the DSC thermogram of gelatin, an endothermal transition from 70 °C to 80 °C was attributed to its glass transition temperature. Endotherms at 110 °C–114 °C and 289 °C–296 °C represented the melting and degradation, respectively, of gelatin.[38] The thermal scan of the SLN loaded polymeric formulation displayed endotherms at 59 °C and 122 °C–129 °C, indicating the melting point of stearic acid and glass transition temperature of polymeric blend (*i.e.*, chitosan and gelatin), respectively. An endotherm onset after 300 °C manifested the decomposition of the SLN encapsulated polymeric formulation. Absence of distinctive melting peak of miconazole nitrate suggested its amorphization/solubilization within the prepared formulation.

3.6. X-ray diffraction

XRD scans of prepared drug loaded SLNs, miconazole nitrate SLN incorporated polymeric formulation and their constituents are shown in Fig. 6. Stearic acid displayed two sharp diffraction peaks at 2θ = 20.9° and 23.2°, indicating its crystalline nature.[39] Absence of any diffraction peak in the XRD scan of gelatine represented its amorphous nature.[40] In the XRD scan of chitosan, a peak recorded at 2θ = 19.6° was attributed to its semi-crystalline nature.[41] The XRD scan of miconazole nitrate displayed sharp diffraction peaks at 2θ = 15.7°, 19.5°, 22.7°, 23.4°, 25.4° and 30.6°, confirming its crystalline nature.[42] The

Table 1 Band frequencies in the FTIR spectra of individual components and prepared formulations[22,31–33,37,38,50–52]

IR frequencies/wave number (cm^{-1})								
Stearic acid	Tween 80	Miconazole nitrate	SLNs	Chitosan	Gelatin	PEG 400	SLNs based formulation	Assigned bands
—	1109	1008, 1085	—	1031	1083	1085, 1101	1099	C–O, C–C stretch
1295, 1467	1467	1405, 1473	1291, 1472	—	1245, 1450	1469	1254, 1470	C–H bend
—	—	—	—	1596	1530	—	1545	N–H bend
—	—	1581, 1585	—	—	—	—	—	C=C aromatic
1701	1739	—	1692	—	1637	—	1638	C=O stretch
2844, 2912	2885, 2929	2973, 3102	2845, 2914	2896	2925, 3054	2879	2853, 2914	C–H stretch
—	—	1322, 3185	—	—	—	—	—	C–N stretch
—	—	—	—	3250–3450	—	3400–3450	3220–3340	O–H stretch

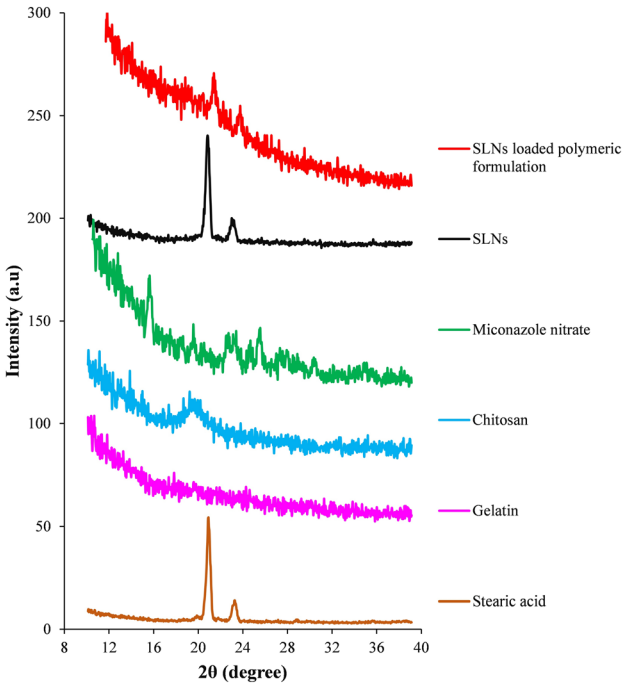

Fig. 6 X-ray diffraction scans of individual constituents, prepared miconazole nitrate SLNs and SLN loaded polymeric formulation.

XRD scan of miconazole nitrate loaded SLNs showed the diffraction peaks of stearic acid. Any sharp diffraction peak of the crystalline drug was not observed, thus suggesting the existence of miconazole nitrate within the lipidic nanoparticles in an amorphous state. XRD scan of the miconazole nitrate SLN incorporated polymeric formulation exhibited peaks at 2θ = 21.3° and 23.6°, indicating the presence of stearic acid. However, the diffraction peaks of chitosan and miconazole nitrate were absent, suggesting their amorphization.

3.7. Mechanical properties

Formulations BF and MF showed tensile strengths of 0.0217 ± 0.0026 MPa and 0.0218 ± 0.0030 MPa, respectively. The SF exhibited a relatively lower tensile strength, *i.e.*, 0.0161 ± 0.0021 MPa as compared to the BF and MF (Fig. 7). An ~1.35 times reduction in the tensile strength was observed due to the inclusion of stearic acid-based SLNs in the polymeric formulation.

3.8. *In vitro* drug release study

The *in vitro* release profiles of prepared formulations, *i.e.*, MF, SF and SP are shown in Fig. 8. The MF showed 64.60 ± 2.12% release of miconazole nitrate in the first 15 minutes, while a maximum drug release, *i.e.*, 94.40 ± 4.5% was observed over 80 minutes. The SF and SP displayed 23.06 ± 5.61% and 28.92 ± 7.02% drug release, respectively, in the first 15 minutes. The release of the drug almost doubled within the next 15 minutes and reached 92.85 ± 2.19% and 93.92 ± 3.21% for the SF and SP, respectively, over 150 minutes. A relatively higher release (~6%) of the drug from the SP as compared to the SF, in the

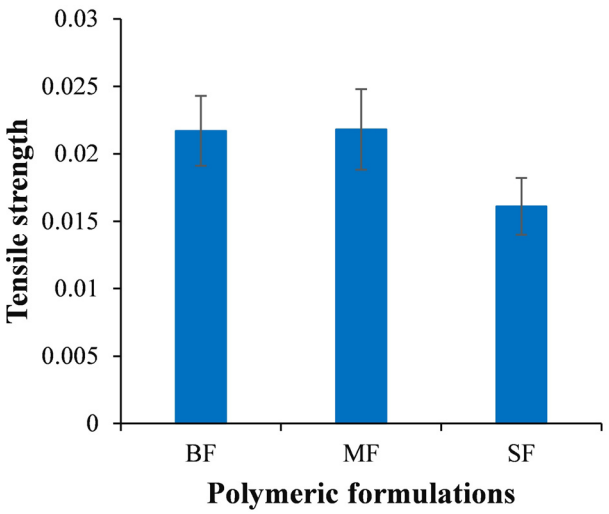

Fig. 7 Tensile strength exhibited by different polymeric formulations.

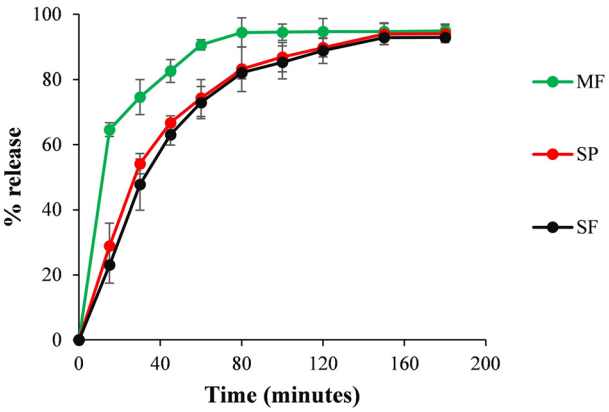

Fig. 8 *In vitro* release profile of miconazole nitrate from the pure antifungal agent loaded polymeric film (MF), SLN loaded polymeric film (SF) and MN patch(SP).

first 15 minutes, was possibly due to rapid dissolution of micron-sized projections of the patch. SLN-based polymeric formulations provided release of the anti-fungal agent for a significantly prolonged duration (*i.e.*, almost double) as compared to the pure miconazole nitrate loaded formulation (one sample *t*-test, $p < 0.05$) due to incorporation of the drug within the lipidic core.

Dissolution modelling results indicated (on the basis of R^2 value) that the drug release profile of the MF followed the Korsmeyer-Peppas model with an '*n*' value of 0.148, indicating the involvement of the Fickian diffusion process, while SLN-based formulations followed first order kinetics.

3.9. *In vitro* anti-biofilm activity

Reduction (%) in the mass of fungal biofilm following BF, MS, SF and SP treatment is shown in Fig. 9I. Any notable decrease in the mass of biofilm was not observed following BF treatment (only 3.06 ± 0.9%). The MS treated biofilm showed a

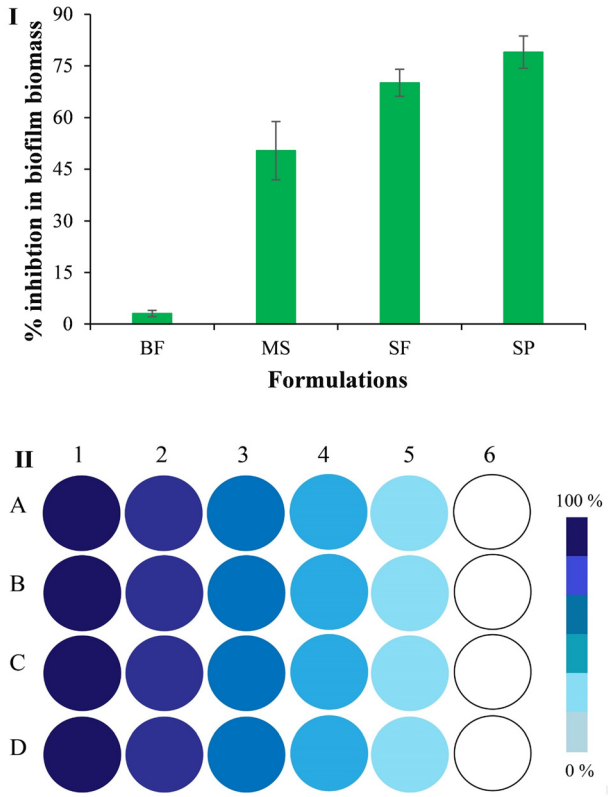

Fig. 9 (I) % Inhibition of the biomass of *C. albicans* biofilm treated using the BF (blank film), MS (aqueous suspension of miconazole nitrate), SF and SP (SLN loaded film and MN patch, respectively). (II) Schematic representation of biofilm developed wells (1) untreated and treated using (2) the BF, (3) MS, (4) SF and (5) SP (gradually decreasing color intensity indicates a reduction in the mass of fungal biofilms).

50.35 ± 8.5% decrease in biofilm mass. Biofilms treated using the SF and SP exhibited a 70.12 ± 3.9% and 78.96 ± 4.7% reduction, respectively, in their mass, suggesting the anti-biofilm activity of the prepared formulations against *C. albicans*. The statistical analysis of data by a one sample *t*-test indicated a significant difference ($p < 0.05$) in the anti-biofilm activity of MS and SLNS-based formulations. The particle loaded formulations showed a higher anti-biofilm activity due to amorphization of miconazole nitrate, its incorporation within nano-scaled lipidic carriers (capable of penetrating the extracellular polymeric substance of biofilms[43]) and polymeric formulation prepared using gelatin and chitosan (which is reported to exhibit anti-fungal potential[44]). Amongst SLN loaded formulations, the SP showed a significantly higher ($p < 0.05$) anti-biofilm activity than the SF because the micron-scaled needles delivered anti-fungal incorporated SLNs into deep biofilm layers (Fig. 9II).

3.10. *In vivo* anti-biofilm activity

On the 3rd day of incision, the skin tissues at the site of injury appeared inflamed. Microscopic examination of the swab sample revealed that the pathogen found in the wound was *C. albicans* (Fig. 10A), thus confirming the development of fungal biofilm. Physical images of the infected site, captured regularly, are depicted in Table 2.

During the first 2 days of treatment, the infected area of all treatment groups appeared swollen. On day 4 of treatment, a reduction in swelling was observed in groups BF, MS and SF. In the case of group SP, any inflammation was not observed. The wound size was reduced by 18%, 5%, 25% and 43% in groups BF, MS, SF and SP, respectively. On day 6, any inflammation was not visible in all the treatment groups. A 24%, 40%, 50% and 60% reduction in wound size was recorded in groups BF, MS, SF and SP, respectively. Further reduction in wound size was not observed in groups BF and MS on day 8, while groups SF and SP showed a closed incision interface; however, wound scars were visible. On day 10, groups BF and MS exhibited injured skin. In comparison, groups SF and SP showed skin regeneration.

During the first 4 days of treatment, *C. albicans* was present in the wounds of all treatment groups. On day 6, microscopic examination of the swab sample indicated the presence of pathogens in groups BF and MS, while in the cases of groups SF and SP, absence of *C. albicans* confirmed its eradication

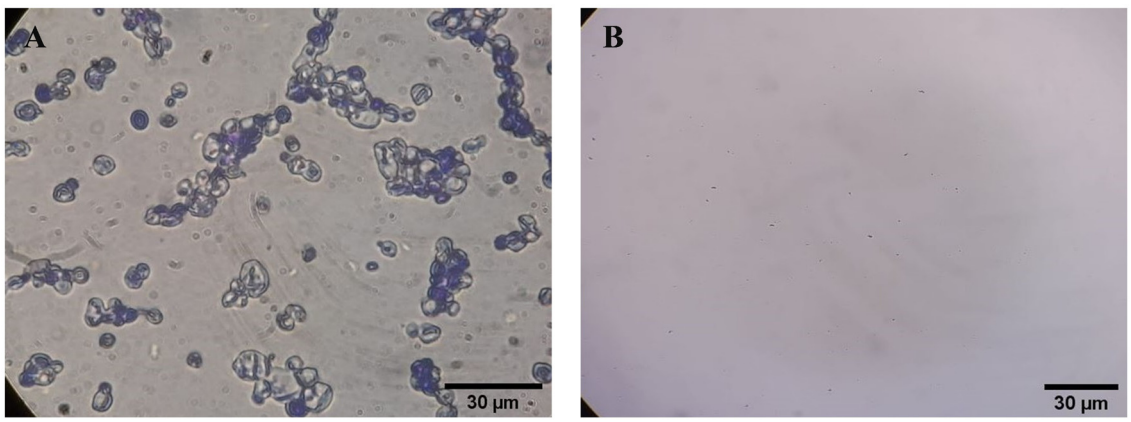

Fig. 10 Representative microscopic images of the swab sample from the wound confirming (A) the presence and (B) absence of *C. albicans*.

Table 2 Images of infected wounds treated using several formulations, *i.e.*, BF, MS, SF and SP on different days

Day	BF	MS	SF	SP
1	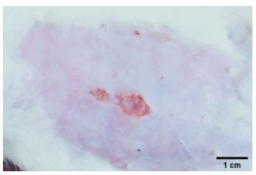	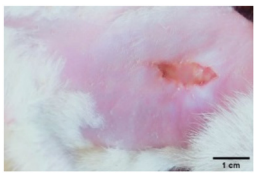	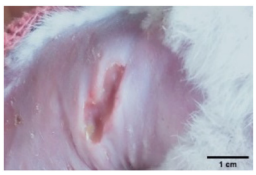	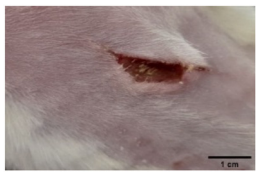
2			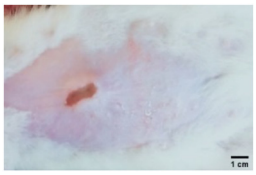	
4	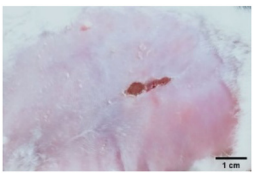		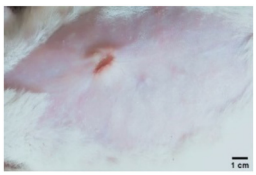	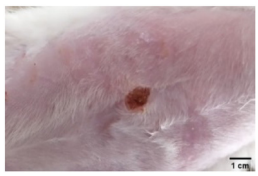
6		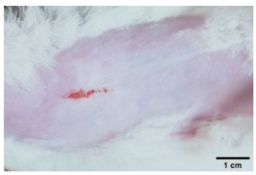		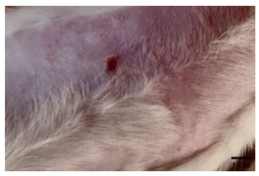
8				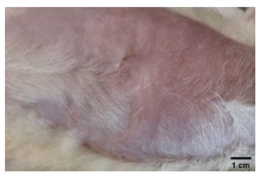
10		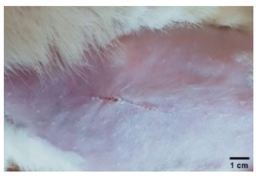		

(Fig. 10B). On day 8, the swab test was negative in groups BF and MS, which suggested eradication of *C. albicans*.

Representative histological images of normal, injured and BF, MS, SF, SP treated skin tissues are shown in Fig. 11. The skin layers including the epidermis and dermis were intact in the normal (without injury and treatment) skin sample. On day 1, the epidermis, connective tissue and blood vessels were damaged in the injured tissue, while the dermis was absent. On day 6 of treatment, the skin layers, connective tissue and blood vessels were underdeveloped in BF, MS and SF treated groups. The SP treated skin sample showed developed blood vessels and connective tissue; however, the skin layers were disrupted. By day 10 of treatment, BF and MS treated skin displayed developed epidermis and connective tissue; however, the dermis was still in the early stage of development. The SF treated group exhibited developed epidermis and dermis with minute disruptions, while SP treated skin was regenerated.

4. Discussion

Globally, fungal infections are estimated to be responsible for over 1.5 million casualties per annum. Around 1 billion people are reported to suffer from cutaneous fungal infections.[45,46] An efficient delivery of anti-fungal agents to the deep cutaneous fungal biofilm by conventional topical (*e.g.*, ointments, gels, lotions, *etc.*) and systemic preparations remains a challenge due to the barrier extracellular polymeric substance, necrotic tissue and poor blood supply to the site of injury. SLNs can serve as suitable candidates for delivering antimicrobial agents to the injured and inflamed skin due to their lipidic nature, which accelerates tissue regeneration.[47] MN mediated delivery of miconazole nitrate loaded lipidic nanoparticles can possibly overcome the above-stated limitations and facilitate on-site (transcutaneous) bioavailability of the encapsulated anti-fungal agent.

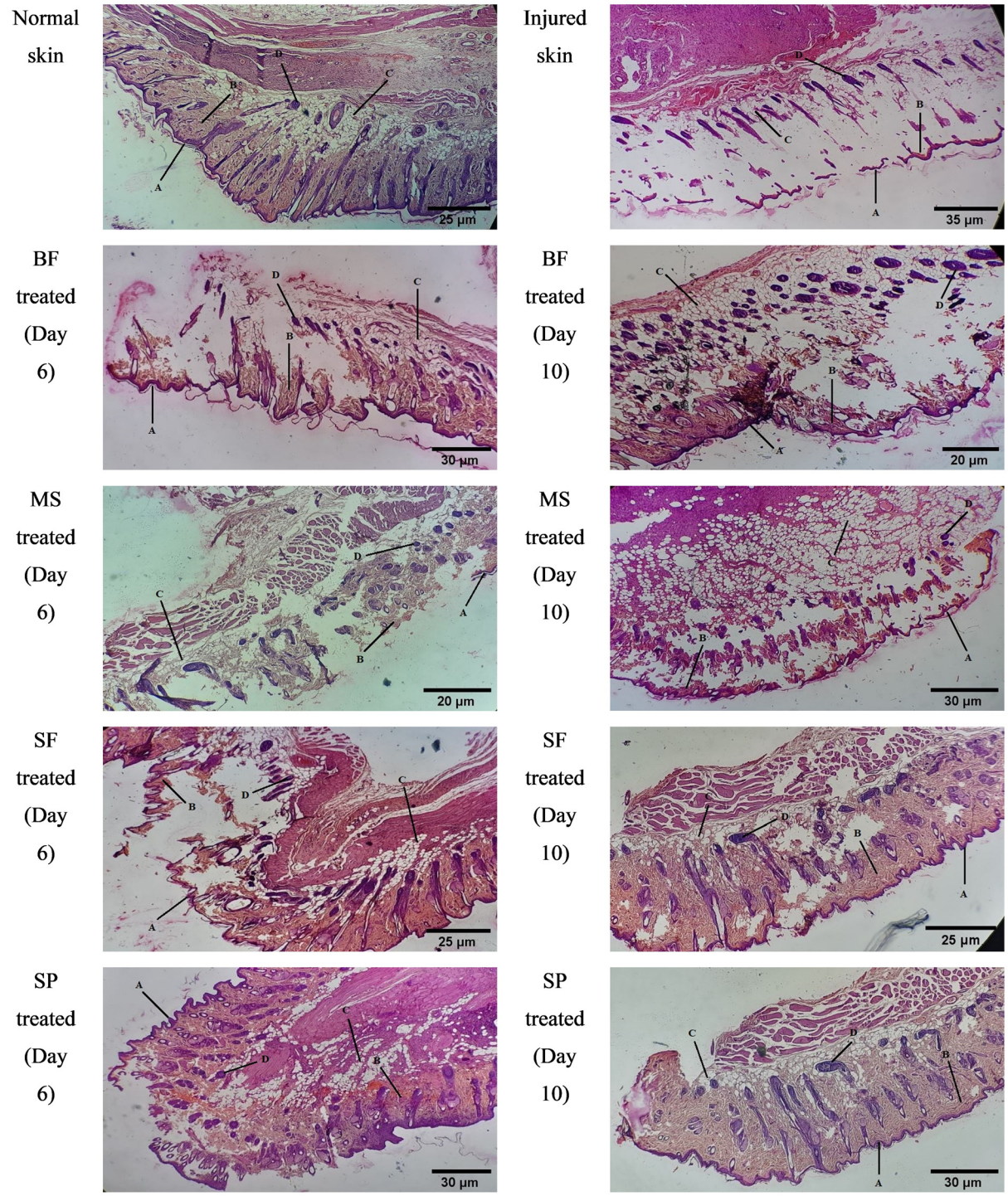

Fig. 11 Representative microscopic images of normal, injured and treated rat skin (A = epidermis, B = dermis, C = connective tissue, and D = blood vessels).

In the present study, miconazole nitrate incorporated stearic acid and Tween 80-based SLNs were prepared by a green manufacturing method (melt emulsification technique), preventing the use of toxic organic solvents. Stearic acid and Tween 80 were used due to their physiologically compatible and non-toxic nature (generally recognized as safe). The fabricated SLNs showed an average diameter of ~224 nm. Literature reports suggest that particles with a diameter ranging from 100 to 400 nm serve as suitable carriers for transcutaneous delivery of therapeutic moieties.[48,49] Chitosan and gelatin were used as base materials for fabricating dissolving MN patches due to their biocompatibility, biodegradability

and film forming ability. Furthermore, chitosan is a reported anti-microbial agent, and hence, serves as a promising carrier for delivering anti-fungal agents to fungal pathogens.[44] Miconazole nitrate SLN loaded MN patches (SP) were fabricated by the vacuum micromolding technique. SP exhibited a folding endurance and % swelling of ~300 and ~359%, respectively, suggesting the integrity and water-uptake ability of the prepared formulation. SP displayed evenly positioned needles with pointed tips and efficiently penetrated the flexible skin simulant film. In the DSC thermogram of the SLN based polymeric formulation, the absence of distinctive melting peak of miconazole nitrate indicated its presence within the solidified lipidic matrix in the amorphous state. XRD results complemented the DSC data and confirmed the amorphization of the drug within the solid lipid matrix. The inclusion of miconazole nitrate lipidic nanoparticles into the polymeric formulation (SF) led to a reduced tensile strength (by ~1.35 times) as compared to pure drug loaded (MF) and blank counterparts (BF). The FTIR spectra of the SLN loaded polymeric formulation exhibited the peaks of stearic acid, gelatin and chitosan with slight shifts, suggesting the incorporation of miconazole nitrate, Tween 80, and PEG 400.

SP provided an extended release of the loaded anti-fungal agent (150 minutes) as compared to the pure miconazole nitrate incorporated polymeric formulation (80 minutes) due to the entrapment of the drug within the solid lipid core. During the *in vitro* anti-biofilm study, SP treated *C. albicans* biofilm exhibited a significantly higher reduction, *i.e.*, ~78% in its mass when compared to the SLN loaded polymeric film (SF), *i.e.*, ~70% and aqueous anti-fungal suspension treatment (MS) *i.e.*, ~50%. This was due to the delivery of the drug within the deep biofilm layers by micron-sized needles. After 10 days of treatment, blank polymeric film (BF) and MF treated *C. albicans* infected wounds did not heal. Topically applied MS could not regenerate damaged skin, rapidly, due to its very short residence time and inability to access deep cutaneous sites. The skin layers of SF applied wounds were relatively less damaged, but were not completely developed after 10 days of treatment. SF showed a relatively better performance than MS due to the loading of miconazole nitrate into the lipidic nanoparticles, which increased the residence time of the antifungal agent; however, the drug could not reach the deep seated biofilm. SP treated infected wounds were healed and displayed developed skin structures. The reasons for this higher anti-biofilm activity as compared to other treatment groups include an easy access to the microbes present in the deeper skin structures. These results suggested that miconazole nitrate SLN loaded MN patches can be used for the treatment of *C. albicans* biofilms.

5. Conclusion

Miconazole nitrate SLN loaded polymeric MN patches (SP) with desired structural integrity and morphological features were fabricated by employing the vacuum micromolding technique. The SLN loaded polymeric formulation showed a tensile strength of 0.0161 ± 0.0021 MPa. The SP released the incorporated anti-fungal agent within 150 minutes and showed suitable anti-biofilm activity *in vitro*. *C. albicans* infected cutaneous wounds were healed after 10 days of treatment with the SP, which indicated that the prepared nanoparticle loaded polymeric MN patches can be used for the treatment of fungal biofilms.

Author contributions

Muhammad Sohail Arshad: conceptualization, writing – original draft, writing – review and editing. Aqsa Ayub: investigation, formal analysis, writing – original draft. Saman Zafar: investigation, formal analysis, writing – original draft. Sadia Jafar Rana: investigation, formal analysis, writing – original draft. Syed Aun Muhammad: writing – original draft, writing – review and editing. Ambreen Aleem: writing – original draft, writing – review and editing. Ekhoerose Onaiwu: writing – review and editing. Kazem Nazari: writing – review and editing. Ming-Wei Chang: writing – review and editing. Zeeshan Ahmad: conceptualization, writing – original draft, writing – review and editing.

Data availability

All data have been made available within the manuscript.

Conflicts of interest

The authors declare that they have no known competing financial interests or personal relationships that could have appeared to influence the work reported in this paper.

Acknowledgements

The authors acknowledge the financial support provided by Higher Education Commission of Pakistan under National Research Program for Universities (NRPU) *vide* no.: 7401/Punjab/NRPU/R&D/HEC/2017.

References

1 W. Wang, K. J. Lu, C. H. Yu, Q. L. Huang and Y. Z. Du, Nano-drug delivery systems in wound treatment and skin regeneration, *J. Nanobiotechnol.*, 2019, **17**, 1–15.
2 G. Sandri, M. C. Bonferoni, F. D'Autilia, S. Rossi, F. Ferrari, P. Grisoli, M. Sorrenti, L. Catenacci, C. Del Fante, C. Perotti and C. Caramella, Wound dressings based on silver sulfadiazine solid lipid nanoparticles for tissue repairing, *Eur. J. Pharm. Biopharm.*, 2013, **84**, 84–90.

3 M. S. Arshad, A. T. Zahra, S. Zafar, H. Zaman, A. Akhtar, M. M. Ayaz, I. Kucuk, M. Maniruzzaman, M.-W. M. W. Chang and Z. Ahmad, Antibiofilm effects of macrolide loaded microneedle patches: Prospects in healing infected wounds, *Pharm. Res.*, 2021, **38**, 165–177.
4 A. K. Singh, A. Mukerjee, H. Pandey and S. B. Mishra, Miconazole Nitrate–Loaded Solid Lipid Nanoparticle-Based Hydrogel Ameliorate Candida albicans Induced Mycoses in Experimental Animals, *J. Bionanosci.*, 2022, **12**, 512–526.
5 M. R. Bhalekar, V. Pokharkar, A. Madgulkar, N. Patil and N. Patil, Preparation and evaluation of miconazole nitrate-loaded solid lipid nanoparticles for topical delivery, *AAPS PharmSciTech*, 2009, **10**, 289–296.
6 R. M. Shah, D. S. Eldridge, E. A. Palombo and I. H. Harding, Microwave-assisted microemulsion technique for production of miconazole nitrate- and econazole nitrate-loaded solid lipid nanoparticles, *Eur. J. Pharm. Biopharm.*, 2017, **117**, 141–150.
7 S. Jain, S. K. Jain, P. Khare, A. Gulbake, D. Bansal and S. K. Jain, Design and development of solid lipid nanoparticles for topical delivery of an anti-fungal agent, *Drug Delivery*, 2010, **17**, 443–451.
8 H. Bunjes, Lipid nanoparticles for the delivery of poorly water-soluble drugs, *J. Pharm. Pharmacol.*, 2010, **62**, 1637–1645.
9 A. K. Singh, A. Mukerjee, H. Pandey and S. B. Mishra, Fabrication of solid lipid nanoparticles by hot high shear homogenization and optimization by Box—Behnken design: An accelerated stability assessment, *J. Appl. Pharm. Sci.*, 2021, **11**, 035–047.
10 B. M. Aljaeid and K. M. Hosny, Miconazole-loaded solid lipid nanoparticles: Formulation and evaluation of a novel formula with high bioavailability and antifungal activity, *Int. J. Nanomed.*, 2016, **11**, 441–447.
11 S. Kumar and J. K. Randhawa, Solid lipid nanoparticles of stearic acid for the drug delivery of paliperidone, *RSC Adv.*, 2015, **5**, 68743–68750.
12 I. L. Dantas, K. T. S. Bastos, M. Machado, J. G. Galvão, A. D. Lima, J. K. M. C. Gonsalves, E. D. P. Almeida, A. A. S. Araújo, C. T. de Meneses, V. H. V. Sarmento, R. S. Nunes and A. A. M. Lira, Influence of stearic acid and beeswax as solid lipid matrix of lipid nanoparticles containing tacrolimus, *J. Therm. Anal. Calorim.*, 2018, **132**, 1557–1566.
13 C. Kriegel, M. Festag, R. S. K. Kishore, D. Roethlisberger and G. Schmitt, Pediatric safety of polysorbates in drug formulations, *Children*, 2020, **7**, 1–12.
14 H. Zhang, M. Yao, R. A. Morrison and S. Chong, Commonly used surfactant, Tween 80, improves absorption of P-glycoprotein substrate, digoxin, in rats, *Arch. Pharmacal Res.*, 2003, **26**, 768–772.
15 A. K. Hassan, Effective surfactants blend concentration determination for o/w emulsion stabilization by two nonionic surfactants by simple linear regression, *Indian J. Pharm. Sci.*, 2015, **77**, 461–469.
16 A. Prabhu, J. Jose, L. Kumar, S. Salwa, M. Vijay Kumar and S. M. Nabavi, Transdermal Delivery of Curcumin-Loaded Solid Lipid Nanoparticles as Microneedle Patch: an In Vitro and In Vivo Study, *AAPS PharmSciTech*, 2022, **23**, 1–12.
17 M. S. Arshad, S. Zafar, A. T. Zahra, M. H. Zaman, A. Akhtar, I. Kucuk, M. Farhan, M. W. Chang and Z. Ahmad, Fabrication and characterisation of self-applicating heparin sodium microneedle patches, *J. Drug Targeting*, 2020, **29**, 60–68.
18 V. T. Arantes, A. A. G. Faraco, F. B. Ferreira, C. A. Oliveira, E. Martins-Santos, P. Cassini-Vieira, L. S. Barcelos, L. A. M. Ferreira and G. A. C. Goulart, Retinoic acid-loaded solid lipid nanoparticles surrounded by chitosan film support diabetic wound healing in in vivo study, *Colloids Surf., B*, 2020, **188**, 110749.
19 S. A. Mathew and S. Arumainathan, Crosslinked Chitosan-Gelatin Biocompatible Nanocomposite as a Neuro Drug Carrier, *ACS Omega*, 2022, **7**, 18732–18744.
20 N. S. Said and N. M. Sarbon, Physical and Mechanical Characteristics of Gelatin-Based Films as a Potential Food Packaging Material: A Review, *Membranes*, 2022, **12**, 1–26.
21 T. P. Singh, M. K. Chatli and J. Sahoo, Development of chitosan based edible films: process optimization using response surface methodology, *J. Food Sci. Technol.*, 2015, **52**, 2530–2543.
22 M. A. Marcos, D. Cabaleiro, M. J. G. Guimarey, M. J. P. Comuñas, L. Fedele, J. Fernández and L. Lugo, PEG 400-based phase change materials nano-enhanced with functionalized graphene nanoplatelets, *Nanomaterials*, 2018, **8**, 1–18.
23 J. Kim and P. Sudbery, Candida albicans, a major human fungal pathogen, *J. Microbiol.*, 2011, **49**, 171–177.
24 J. Gil, M. Solis, A. Higa and S. C. Davis, Candida albicans Infections: a novel porcine wound model to evaluate treatment efficacy, *BMC Microbiol.*, 2022, **22**, 1–9.
25 C. Dumont, S. Bourgeois, H. Fessi, P. Y. Dugas and V. Jannin, *In vitro* evaluation of solid lipid nanoparticles: Ability to encapsulate, release and ensure effective protection of peptides in the gastrointestinal tract, *Int. J. Pharm.*, 2019, **565**, 409–418.
26 U. Jillani, J. Mudassir, M. S. Arshad, P. Mehta, Y. Alyassin, K. Nazari, B. Yousef, M. Patel, A. Zaman, E. Sayed, M. W. Chang, A. Ali and Z. Ahmad, Design and evaluation of agarose based buccal films containing zolmitriptan succinate: Application of physical and chemical enhancement approaches, *J. Drug Delivery Sci. Technol.*, 2022, **69**, 103041.
27 Y. Jin, H. K. Yip, Y. H. Samaranayake, J. Y. Yau and L. P. Samaranayake, Biofilm-forming ability of Candida albicans is unlikely to contribute to high levels of oral yeast carriage in cases of human immunodeficiency virus infection, *J. Clin. Microbiol.*, 2003, **41**, 2961–2967.
28 A. S. Melo, F. C. Bizerra, E. Freymüller, B. A. Arthington-Skaggs and A. L. Colombo, Biofilm production and evaluation of antifungal susceptibility amongst clinical Candida spp. isolates, including strains of the Candida parapsilosis complex, *Med. Mycol.*, 2011, **49**, 253–262.

29 H. T. Taff, J. E. Nett and D. R. Andes, Comparative analysis of Candida biofilm quantitation assays, *Med. Mycol.*, 2012, **50**, 214–218.
30 J. C. Garber, R. W. Barbee, J. T. Bielitzki, L. A. Clayton, J. C. Donovan, D. F. Kohn, N. S. Lipman, P. Locke, J. Melcher, F. W. Quimby, P. V. Turner, G. A. Wood and H. Wurbel, *Guide for the Care and Use of Laboratory Animals*, National Research Council, National Academies Press, 8th edn, 2011.
31 M. Qushawy, A. Nasr, M. Abd-Alhaseeb and S. Swidan, Design, optimization and characterization of a transfersomal gel using miconazole nitrate for the treatment of candida skin infections, *Pharmaceutics*, 2018, **10**, 1–23.
32 A. A. Al-Badr, Miconazole Nitrate: Comprehensive Profile, *Profiles Drug Subst., Excipients, Relat. Methodol.*, 2005, **32**, 1–66.
33 H. A. Ebrahimi, Y. Javadzadeh, M. Hamidi and M. B. Jalali, Repaglinide-loaded solid lipid nanoparticles: Effect of using different surfactants/stabilizers on physicochemical properties of nanoparticles, *Daru, J. Pharm. Sci.*, 2015, **23**, 1–11.
34 C. Li, B. Xie, J. Chen, Z. Chen, X. Sun and S. W. Gibb, H_2O_2-microwave treated graphite stabilized stearic acid as a composite phase change material for thermal energy storage, *RSC Adv.*, 2017, **7**, 52486–52495.
35 N. Ahmad, R. Ahmad, A. Al-Qudaihi, S. E. Alaseel, I. Z. Fita, M. S. Khalid and F. H. Pottoo, Preparation of a novel curcumin nanoemulsion by ultrasonication and its comparative effects in wound healing and the treatment of inflammation, *RSC Adv.*, 2019, **9**, 20192–20206.
36 J. Y. Fang, C. L. Fang, C. H. Liu and Y. H. Su, Lipid nanoparticles as vehicles for topical psoralen delivery: Solid lipid nanoparticles (SLN) versus nanostructured lipid carriers (NLC), *Eur. J. Pharm. Biopharm.*, 2008, **70**, 633–640.
37 S. Acosta-Ferreira, O. S. Castillo, J. T. Madera-Santana, D. A. Mendoza-García, C. A. Núñez-Colín, C. Grijalva-Verdugo, A. G. Villa-Lerma, A. T. Morales-Vargas and J. R. Rodríguez-Núñez, Production and physicochemical characterization of chitosan for the harvesting of wild microalgae consortia, *Biotechnol. Rep.*, 2020, **28**, e00554.
38 D. Kotatha, M. Hirata, M. Ogino, S. Uchida, M. Ishikawa, T. Furuike and H. Tamura, Preparation and Characterization of Electrospun Gelatin Nanofibers for Use as Nonaqueous Electrolyte in Electric Double-Layer Capacitor, *J. Nanotechnol.*, 2019, **2019**, 1–11.
39 Y. Chen, X. Zhang, B. Wang, M. Lv, Y. Zhu and J. Gao, Fabrication and characterization of novel shape-stabilized stearic acid composite phase change materials with tannic-acid-templated mesoporous silica nanoparticles for thermal energy storage, *RSC Adv.*, 2017, **7**, 15625–15631.
40 M. S. Arshad, S. Zafar, S. J. Rana, K. Nazari, M. W. Chang and Z. Ahmad, Fabrication of gentamicin sulphate laden stimulus responsive polymeric microarray patches for the treatment of bacterial biofilms, *J. Drug Delivery Sci. Technol.*, 2023, **84**, 104504.
41 Z. Jia, C. Yang, F. Zhao, X. Chao, Y. Li and H. Xing, One-step reinforcement and deacidification of paper documents: Application of Lewis base—chitosan nanoparticle coatings and analytical characterization, *Coatings*, 2020, **10**, 1–15.
42 G. Tejada, N. L. Calvo, M. Morri, M. Sortino, C. Lamas, V. A. Álvarez and D. Leonardi, Miconazole nitrate microparticles in lidocaine loaded films as a treatment for oropharyngeal candidiasis, *Materials*, 2023, **16**, 1–14.
43 P. Kaiser, J. Wächter and M. Windbergs, Therapy of infected wounds: overcoming clinical challenges by advanced drug delivery systems, *Drug Delivery Transl. Res.*, 2021, **11**, 1545–1567.
44 P. Y. Shih, Y. T. Liao, Y. K. Tseng, F. S. Deng and C. H. Lin, A potential antifungal effect of chitosan against candida albicansis mediated via the inhibition of SAGA complex component expression and the subsequent alteration of cell surface integrity, *Front. Microbiol.*, 2019, **10**, 1–14.
45 K. Urban, S. Chu, C. Scheufele, R. L. Giesey, S. Mehrmal, P. Uppal and G. R. Delost, The global, regional, and national burden of fungal skin diseases in 195 countries and territories: A cross-sectional analysis from the Global Burden of Disease Study 2017, *JAAD Int.*, 2021, **2**, 22–27.
46 E. Rayens and K. A. Norris, Prevalence and Healthcare Burden of Fungal Infections in the United States, 2018, *Open Forum Infect. Dis.*, 2022, **9**, 1–12.
47 F. Motsoene, H. Abrahamse and S. S. D. Kumar, Multifunctional lipid-based nanoparticles for wound healing and antibacterial applications: A review, *Adv. Colloid Interface Sci.*, 2023, **321**, 103002.
48 B. C. Palmer and L. A. DeLouise, Nanoparticle-enabled transdermal drug delivery systems for enhanced dose control and tissue targeting, *Molecules*, 2016, **21**, 1–17.
49 E. Subroto, R. Andoyo and R. Indiarto, Solid Lipid Nanoparticles: Review of the Current Research on Encapsulation and Delivery Systems for Active and Antioxidant Compounds, *Antioxidants*, 2023, **12**, 1–28.
50 J. Peng, X. Wang and T. Lou, Preparation of chitosan/gelatin composite foam with ternary solvents of dioxane/acetic acid/water and its water absorption capacity, *Polym. Bull.*, 2020, **77**, 5227–5244.
51 F. Badria and E. Mazyed, Formulation of nanospanlastics as a promising approach for improving the topical delivery of a natural leukotriene inhibitor (3-acetyl-11-keto-β-boswellic acid): Statistical optimization, in vitro characterization, and ex vivo permeation study, *Drug Des., Dev. Ther.*, 2020, **14**, 3697–3721.
52 K. Pramod, C. V. Suneesh, S. Shanavas, S. H. Ansari and J. Ali, Unveiling the compatibility of eugenol with formulation excipients by systematic drug-excipient compatibility studies, *J. Anal. Sci. Technol.*, 2015, **6**, 1–14.